10-2022

# Increased Panel Height Enhances Cooling for Photovoltaic Solar Farms

Sarah E. Smith
*Portland State University*

Bianca Viggiano
*Portland State University*, viggiano@pdx.edu

Naseem Ali
*Portland State University*, naseem@pdx.edu

Timothy J. Silverman
*National Renewable Energy Laboratory, Golden*

Martin Obligado
*University Grenoble Alpes*

*See next page for additional authors*



## Citation Details

Smith, S. E., Viggiano, B., Ali, N., Silverman, T. J., Obligado, M., Calaf, M., & Cal, R. B. (2022). Increased panel height enhances cooling for photovoltaic solar farms. Applied Energy, 325, 119819.

Applied Energy 325 (2022) 119819

Contents lists available at ScienceDirect

Applied Energy

journal homepage: www.elsevier.com/locate/apenergy

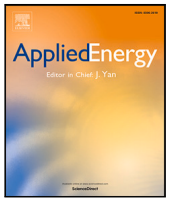

# Increased panel height enhances cooling for photovoltaic solar farms

Sarah E. Smith [a], Bianca Viggiano [a], Naseem Ali [a], Timothy J Silverman [c], Martín Obligado [d], Marc Calaf [b], Raúl Bayoán Cal [a,*]

[a] Department of Mechanical and Materials Engineering, Portland State University, Portland, OR 97207, USA
[b] Department of Mechanical Engineering, University of Utah, Salt Lake City, UT 84112, USA
[c] National Renewable Energy Laboratory (NREL), Golden, CO 80401, USA
[d] Université Grenoble Alpes, CNRS, Grenoble-INP, LEGI, F-38000 Grenoble, France

ARTICLE INFO

*Keywords:*
Solar farms
Convective heat transfer
Experimental fluid dynamics
Photovoltaic
Turbulence

ABSTRACT

Solar photovoltaic (PV) systems suffer substantial efficiency loss due to environmental and internal heating. However, increasing the canopy height of these systems promotes surface heat transfer and boosts production. This work represents the first wind tunnel experiments to explore this concept in terms of array flow behavior and relative convective heat transfer, comparing model solar arrays of varied height arrangements - a nominal height, extended height, and a staggered height configuration. Analyses of surface thermocouple data show average Nusselt number ($Nu$) to increase with array elevation, where panel convection at double height improved up to 1.88 times that of the nominal case. This behavior is an effect of sub-array entrainment of high velocity flow and panel interactions as evidenced through flow statistics and mean kinetic energy budgets on particle image velocimetry (PIV) data. The staggered height arrangement encourages faster sub-panel flow than in the nominal array. Despite sub-array blockage due to the lower panel interaction, heat shedding at panel surfaces promotes improvements on $Nu$ over 1.3 times that of the nominal height case.

## 1. Introduction

As renewable energy sources increase in global prevalence, solar photovoltaic (PV) collection is becoming a key contributor to installed generation capacity [1]. In the U.S., the warm and sunny states of California, Arizona and Texas contribute more than 50% of the nation's utility-scale solar electricity generation [2]. High solar intensity and increased ambient temperatures in these regions raise PV panel temperatures, in turn reducing module efficiency [3–5]. Even modules situated in more temperate climates like Colorado are at risk where summer air temperatures of higher than 35 °C can heat panels up to 60 °C [6]. Common PV unit operating temperatures between 45 °C and 65 °C translate to 20 °C and 40 °C higher than their rated standard test condition (STC) temperature of 25 °C [7]. In this range, commonly used silicon solar cells can lose efficiency up to 0.5% per degree above STC and incur up to 12% in efficiency losses [5]. Many available active cooling methods induce higher convective heat transfer, including fans/blowers and induced latent heat or phase change [e.g. 8–11]. But all these solutions often require external power and resources such as water, making passive cooling methods such as wind-driven convection much more desirable.

Recently, PV farms have begun to incorporate mixed-use designs with agricultural practices, where raised panels allow land below the array to be used for grazing animals and crops which benefit from the intermittent shade [12–14]. These 'agrivoltaic' sites encourage greater module cooling due to natural evaporative interactions and transpiration from the plants below, suggesting that these spaces might also benefit from increased module height [15,16]. Studies show that these such systems may actually assist the vegetation, where shade from the modules limit light and over-heating. This effect in turn reduces the amount of water removed from the plants, ultimately decreasing the amount of irrigation needed [17,18].

Much like urban and vegetation canopies, flow within a solar PV array interacts with the panels, trapping or diverting energy, and complicating the relation between heat transfer and the external passing flow [19]. Approaching solar arrays as canopy flow is a relatively new venture. Recent work by Stanislawski [20] discussed that panel arrangement has significant influence on convective heat transfer within solar arrays, where LES simulations on a three-dimensional (3D) array found improvements on convective coefficient $h$ of 14.8% based on array pattern. Other modifications such as tilt angle and inflow direction introduce variations in panel surface cooling by modifying wind-module interactions. For example, Glick et al. [21] observed convective cooling increases between 30% and 45% when modules

* Corresponding author.
*E-mail address:* rcal@pdx.edu (R.B. Cal).

https://doi.org/10.1016/j.apenergy.2022.119819
Received 16 March 2022; Received in revised form 13 July 2022; Accepted 7 August 2022
Available online 29 August 2022

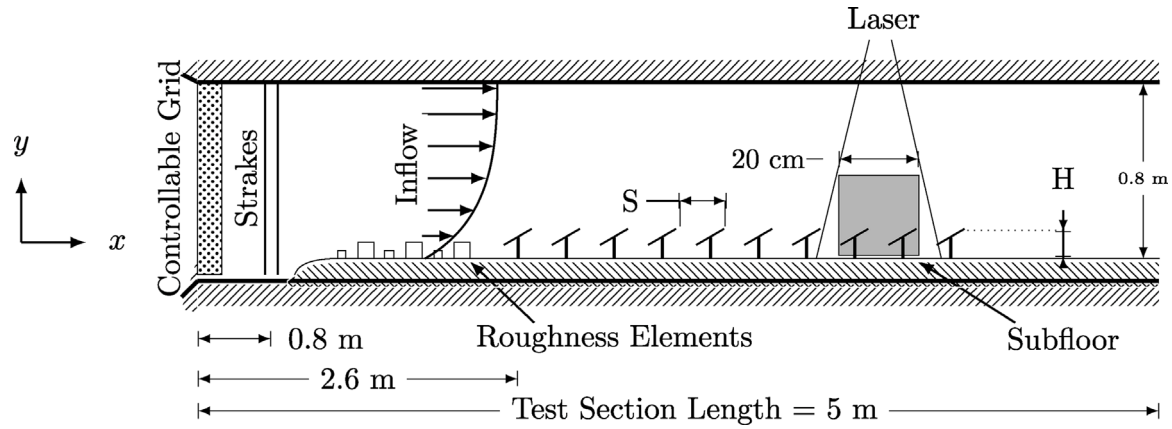


**Fig. 1.** Schematic of experimental facility and farm arrangement for nominal (NM) $H = 63.4$ mm case as adapted from Glick et al. [21]. A span of $S = 1.4H$ from trailing edge to trailing edge separates array rows.

were oriented −30° with respect to oncoming flow *versus* their +30° counterparts, increasing the volume of high velocity flow pulled into the array. Such arrangements are common in operating PV systems where wind orientation is highly varied, and in modern variable-tilt systems which change inclination to optimize for sun position. These variations, coupled with irregular wind direction, have consequences on physical wind loading [22]. Thus, optimized design requires a balanced tradeoff between increased cooling, maximized solar incidence, and possible increases in damage to module structures.

For PV units, the subject of forced convection on individual inclined plates has been well-researched, including wind-forced convection on heated plates [23,24], and both roof-mounted and free-standing panels [25–27]. Generally, the above studies aim to relate the convective heat transfer coefficient $h$ of simple plates to minimal parameters such as inflow velocity, plate geometry/arrangement, plate orientation, and turbulent inflow conditions [23,24,27–30]. However, the plate-scale investigation is unable to fully describe the canopy-like flow observed for full solar arrays, particularly when considering effects of module height on module cooling [31,32]. Performing field experiments in large-scale PV farms is difficult due to limited accessibility toward setting thermal and velocity measurement devices, requiring sensor placement in non-ideal locations [33]. Without precise surface temperatures, heat transfer correlations become increasingly complex and difficult to apply to real world sites [34,35]. Models created to overcome these limitations commonly simplify the system to correlations based on irradiance, temperature, and wind speed [35]. Energy-based models aim to predict surface temperature by estimating the more elusive quantities such as radiation, but are inherently reliant on pre-defined and embedded panel material properties [36]. These surface-level approaches help to understand small-scale physics for individual PV panels, but zooming out reveals a complex canopy whose physics vary with the placement of objects within.

The present work approaches industrial solar farm design from a uniquely interdisciplinary context. While previous works explored configurations changes such as inclination and spacing, this study is understood by the authors to be the first work investigating sub-panel flow energetically and relative convection benefits based on altered PV array height. Blending heat transfer theory and energetic fluid mechanics, this new perspective on PV convection research investigates the role of solar panel elevation on module cooling from the viewpoint of full-farm energetic flow interactions. In this work, we identify and discuss the physical phenomena responsible for PV panel cooling as it pertains to wind interaction throughout solar farm canopies. A scaled model of an operating solar farm was modified to represent three panel height configurations: all modules set to a nominal mount height (NM), all high mounting (HM), and a staggered arrangement (SM) alternating NM and HM throughout. Our multifaceted approach to examining these spaces will pave the way for more efficient farm designs, tailored to unique spatial, agricultural, and environmental constraints with minimal added cost in terms of farm construction.

Expanding analysis beyond the panel surface, we capture differences in turbulent flow behavior within and around the farm using particle image velocimetry (PIV). This unique vantage point of sub-array mechanics reveals that panel height dictates flow field physics and heat shedding as discussed in terms of mean flow statistics. Quadrant analysis shows that turbulent heat shedding aligns with sweep and ejection events for the shortest and tallest arrangements (NM and HM). Connecting these quantities to the mean kinetic energy (MKE) budget completes the link between heat transfer and flow effects, providing a rare understanding of the primary mechanisms responsible for augmented panel cooling with increased array height. Our work thus highlights the cooling benefit of increasing panel height while introducing new analysis methods and insights for large-scale solar farm canopies. Following this advanced framework, future and current PV arrays can be better assessed in terms of heat transfer and flow-panel interactions, ultimately enhancing farm efficiency.

## 2. Materials and methods

Experiments were conducted in the Portland State University wind tunnel, measuring thermal variation at the PV solar panel as well as measuring the velocity components of the flow (Fig. 1). The test facility is a closed-circuit wind tunnel featuring an active grid at the test-section entrance, followed by vertical strakes, with variable size chains positioned as surface roughness elements to induce scaled atmospheric boundary layer flow as described in Glick et al. [21]. Maximum blockage in the 0.8 m × 1.2 m cross-section was calculated from the staggered array configuration (SM) at 4.3%.

The considered model solar farm was distributed in 10 rows and 4 columns as shown in Fig. 2(a). Panel geometry, array configuration, and energy conditions approximate the solar farm at the Denver Federal Center (DFC). The panel length ($L$), and thickness ($th$) were scaled at a ratio of 1:33 to the type of module used at DFC ($L = 50.8$ mm; $th = 5.3$ mm), and set to a 30° angle of attack. The model array spanned a majority of the tunnel width, with each panel column width set to $W = 254$ mm. Schematic for a single module construction is shown as a cross-section in Fig. 2(b). Height at the trailing edge, $H$, for nominal cases is 63.4 mm. For this study, three different configurations were designed and tested at varied inflow and power conditions. Shown in Fig. 3, the three arrangements were the nominal mount (NM) case with the upper, or trailing edge, height of $H_{NM} = H$, the high mount (HM) case with a trailing edge height of $H_{HM} = 1.6H$, and the staggered mount configuration featuring alternating trailing edge heights of $H_{NM}$ and $H_{HM}$. The streamwise spacing between panel rows ($S$) remained

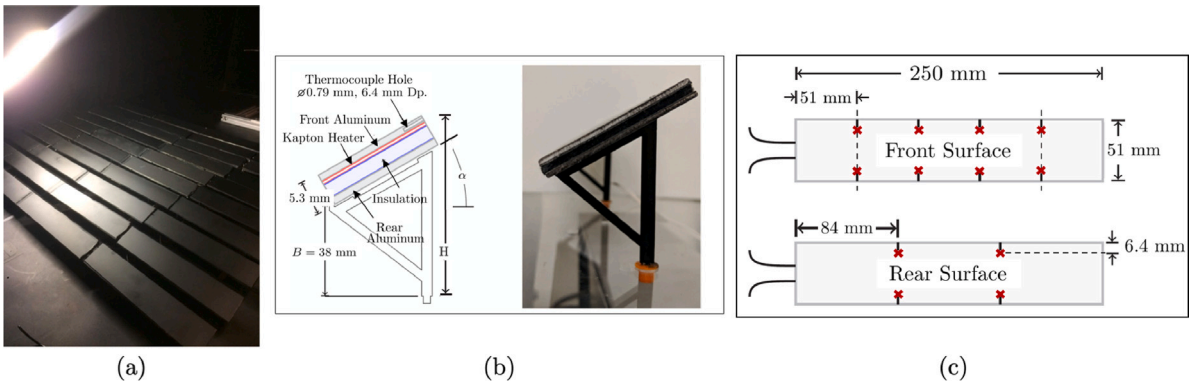


**Fig. 2.** Array model detail: (a) Full wind tunnel array (top-view); (b) Panel construction (side-view); (c) Thermocouple placement at 8th row panel. Images (b) and (c) adapted from Glick et al. [37].

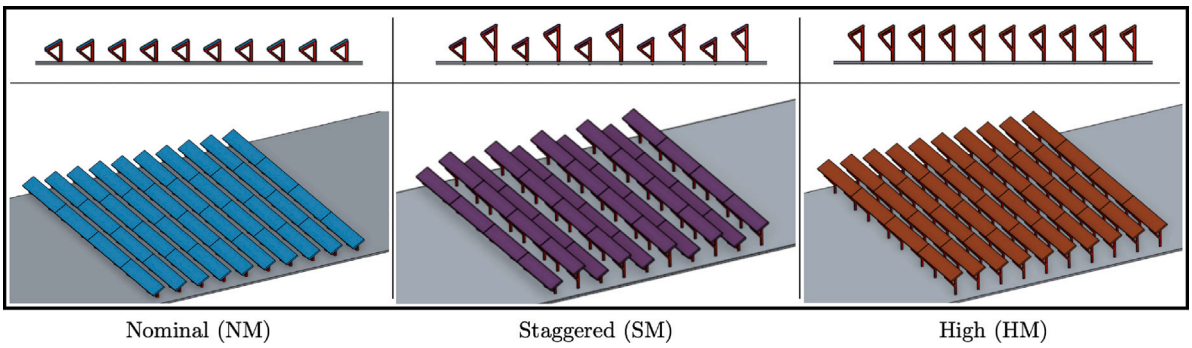


**Fig. 3.** Configurations tested. Nominal (NM) and High (HM) trailing edge (TE) heights are $H_{NM} = H$ and $H_{HM} = 1.6H$, respectively, with Staggered (SM) alternating. Panel colors are set to match profile plots.

consistent at $1.4H_{NM}$ for all cases. Spacing for the SM array is evenly distributed here to simplify analysis to height effects. However, spacing for an operational SM array would be optimized to prohibit shading on lower panels, increasing the distance behind taller rows.

Temperature measurements were taken with thermocouples embedded below the panel surfaces beginning at the 8th row to ensure fully-developed flow states. In the SM case, thermal data were averaged over the 8th and 9th row to encompass both tall and short panel effects, respectively. The panel in row 8 was outfitted with 12 Type $T$ thermocouples: 8 in the front, upward-facing surface and 4 in the rear. Red 'x' locations in Fig. 2(c) show relative positioning projected on both surfaces. Each sensor is secured with thermally conductive silicon in a channel of 0.79 mm diameter at a depth of 6.4 mm as illustrated in Fig. 2(b). The 9th row panel was equipped with a thermocouple on each the front and rear surfaces. An ice-point reference was used to mitigate incidental thermal migration. In all cases, thermal data represent calculations based on averaged values from the 12 surface thermocouples over 5-minute intervals at 30-second increments. Velocity measurements were taken via particle image velocimetry (PIV) between the 8th and 9th panels for NM and HM, as described in Glick et al. [31], and centered on the 9th row for SM. The two-dimension, two-coordinate (2D-2C) system captured data at a resolution of approximately 0.9 mm. Because the measurements rely on a laser sheet projected from above that contacts the physical structures in the flow, some of the domain is subject to shadow and reflection. The vectors reported represent those viable for consideration. All arrangements were tested at different Reynolds number ($Re_L = U_\infty L/\nu_k$) and input heating power, see Table 1. Free stream velocity $U_\infty$ was captured from a pitot tube at a height of 0.4 m, located directly behind the last row of panels. The present discussion is simplified to consider two inflow velocities of $U_\infty \approx 1$ m/s and 4 m/s, representing low and mid-range wind velocities as found in an open environment such as central Arizona [38]. Kinematic viscosity $\nu_k$ is defined based on tabulated values for air at free stream temperature $T_\infty$ taken at the pitot tube location [39]. For more details regarding the tunnel, measurements, and data, the reader is referred to Glick et al. [21,31,37].

**Table 1**
Variable test matrix of inflow and array settings used in experiments. Reynolds number $Re_L$ is based on module length ($Re_L = U_\infty L/\nu_k$).

| $Re_L$ | $U_\infty$ (m/s) | Power (W/m$^2$) | Array height |
|---|---|---|---|
| 3200 | 0.9 | 450 | NM = $H$ |
| 13 000 | 3.9 | 1050 | HM = $1.6H$<br>SM = $H$ and $1.6H$ |

## 3. Results

Thermal and aerodynamic results are presented herein. The thermal analysis characterizes convection via the Nusselt number, $Nu$, emphasizing the effects of array height variation. Furthermore, the aerodynamic analysis of the velocity field presents how the solar PV structures influence the flow, specifically the mean and fluctuating components of velocity. The coupling of flow field velocities and expelled heat from the panel is investigated to quantify the factors that affect velocity deficits and in turn heat transfer near the panel surfaces. Lastly, we discuss the mean kinetic energy budget around the panels, quantifying the physical flow mechanisms responsible for panel heat-shedding.

### 3.1. Thermal results

The Nusselt number describes the convective heat response in comparison to conduction within a moving fluid, and is highly relevant for

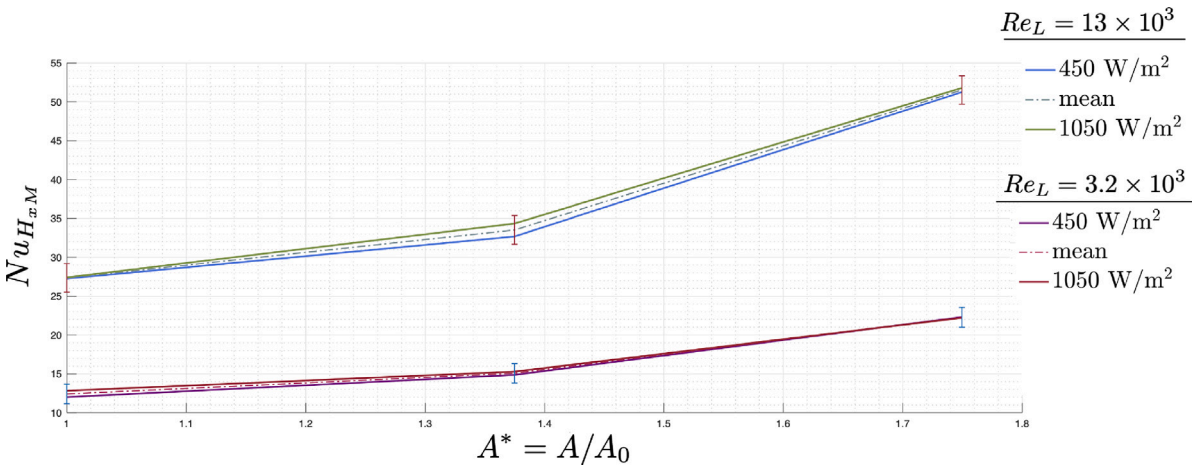


**Fig. 4.** Nusselt number as a function of normalized area, $A^*$. Two mean values of $Re_L$ are included along with two sub-groupings of power inputs.

panel cooling as it considers changes to the thermal properties of the air surrounding the panels. The relative impact of $Re$ and the power input on $Nu$ is presented in Fig. 4. Included is the Nusselt number based on respective canopy height $H_{xM}$ ($Nu = hH_{xM}/k$), plotted as a function of the normalized sub-panel area $A^* = A/A_0$. Sub-panel area $A^*$ is defined as the open space present below a PV module as observed from the side-view projection of an array row. The normalization area $A_0$ is the sub-panel area of NM configuration. Thermal conductivity for air was obtained from empirical tables at $T_\infty$. The convective heat transfer coefficient $h$ was calculated from surface temperature data, acquired from the thermocouples embedded in the panel surfaces. Since thermal data were taken from the front and rear surfaces, an overall convective heat transfer coefficient $h$ was calculated as in Incropera et al. [39] from the two as $h = 1/\left(\frac{1}{h_{front}} + \frac{1}{h_{rear}}\right)$. For each $Re_L$ and area, $A^*$, the mean $Nu$ is provided for comparison. Error bars are presented for the mean values based on uncertainty analysis in Glick et al. [31].

A dependence of the Nusselt number on $Re$ is observed and expected, based on the advecting flow, $U_\infty$. Although less pronounced, a small dependence is also observed based on the power input, signifying that the overall heat transfer and aerodynamic properties should scale with irradiance conditions. Note that power levels of 450 W/m$^2$ and 1050 W/m$^2$ correspond to an irradiance of 43% and 105% of STC rating, respectively.

The notable dependence of $Nu$ is observed as a function of sub-panel area, with $Nu_{H_{HM}}$ improving more than 1.88 times that of $Nu_{H_{NM}}$ as $A^*$ increases from 1 to 1.75. For SM, the more minimal gain of 1.21 times that of $Nu_{H_{NM}}$ suggests that the increase in $Nu_{H_{xM}}$ is primarily a function of canopy height rather than improved convection in the staggered case. This is largely expected to be a consequence of the blocking of sub-array flow by the lower panels, and is further discussed in the following sections where we discuss fluid flow effects. For $Re = 3200$, the change in thermal properties corresponds to a maximum surface temperature decrease of 4.4 °C, and based on literature, corresponds to a gain in power output ranging between 0.5% and 2.25% [40] with lifespan increases of up to 45% at panel temperatures of ~ 60° [41].

### 3.2. Mean flow field statistics

Mean flow statistics, as presented in Fig. 5, highlight the contribution of faster sub-panel flow to the increased convection seen in Section 3.1. The three considered array configurations, NM, SM and HM correspond, respectively, to the left, center and right columns.

The nominal mount (NM) array presents three layers of the flow; an inner layer below the array, an outer layer above the panels and a deficit region which shows heavy blockage by the panels within the array. The velocity magnitude in the inner layer reaches ~30% that of the free stream velocity. Above the panels, a boundary layer is developed and near free stream velocities are reached within the interrogation area. The most complex region lies within the panel array where recirculation occurs following the top tip of the panel. In this region, velocity becomes negative (outlined by the white dashed boundary), reaching a magnitude of 5% of $U_\infty$, in a counterclockwise rotation. The shape of the recirculation zone indicates that flow moves up the panels and therefore the flow recovery is non uniform above the panels. The draft of the fluid off the panels and the pressure differential experienced behind the panels cause an arcing of the contour lines, indication that the wake spreads behind the panels. Since air flow contributes greatly to the convective heat transfer, the front surface is expected to cool more efficiently than the recirculating wake region behind the panel. Uniform gradients of the $U/U_\infty$ are recovered by $y/H \sim 1.5$.

Similar tendencies are observed for the SM array in Fig. 5 (top-middle). The sub-panel velocities are similar in magnitude however the staggered panel heights encourage slower speeds that tend to keep the warmer panel air from moving significantly far from the panels. The wake expansion for the SM array is more prominent than what is observed for NM panels, creating a disparity in heat transfer between the high and the low panels in the array. The HM array provides better cooling due to increased wind speeds below the panel array approaching $U/U_\infty = 65\%$. Furthermore the deficit region within the panels is less pronounced. The HM array provides increased $Nu$ values, as observed in Fig. 4 due to the increased heat-shedding velocities along both the front and rear surfaces of the panels.

Time-averaged wall-normal velocities presented in Fig. 5 (bottom row), provide additional insight into heat transfer mechanisms. The $V/U_\infty$ values for NM and HM demonstrate the majority of the flow is upwards and that downwash occurs from the leading edge and coincides with the front of the array. From the wall, where $V = 0$, flow is quickly positive, drawing the fluid into the recirculation region where $V$ and $U$ are similar in their magnitude in comparison to free stream velocity, $U_\infty$.

At the trailing edge of the NM array panels, a pocket of down-ward flow is present within the wake of the panel, suggesting some pushing of outer flow into the array. The flow then transitions into positive vertical motion as it nears the surface of the following panel. The HM array shows similar trends with slightly increased local velocities, suggesting stronger fluid-to-panel interactions than with the NM case. High levels of vertical flow are observed above the short panels for the SM array. Increased mixing of the fluid is obtained by alternating positive and negative wall-normal velocities as the streamwise fluid weaves between the panels. However, the primarily negative (downward) flow above the shorter panel suggests the flow within this region is kept near to the panels rather than evacuating heat into the outer flow.

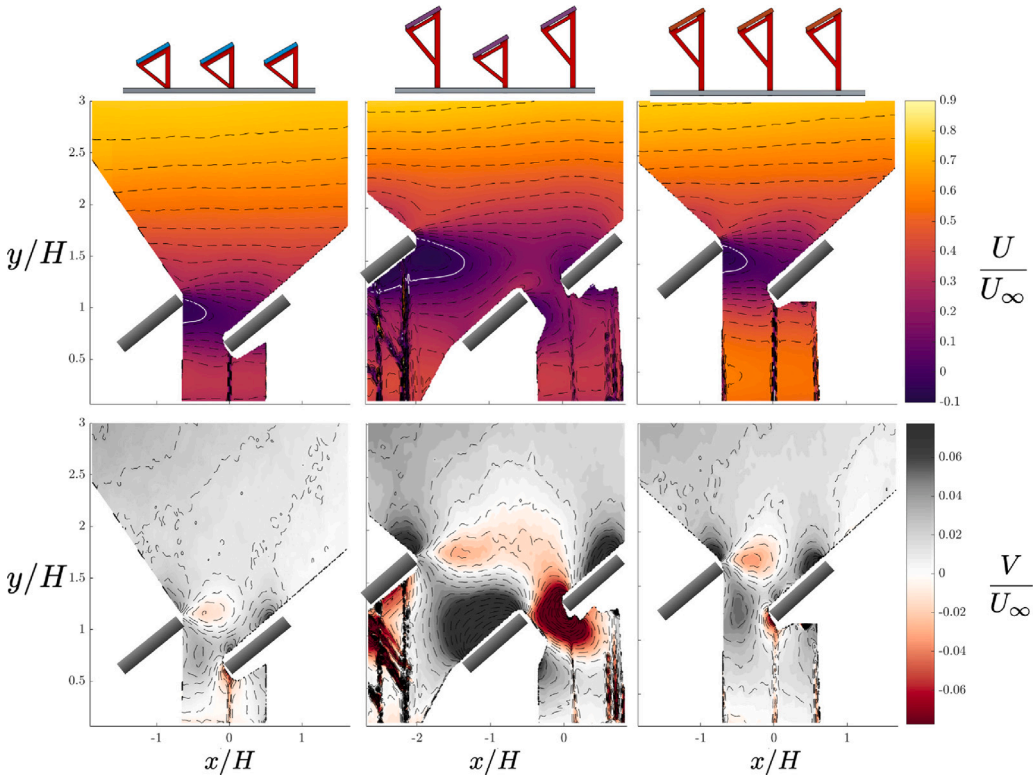


**Fig. 5.** Normalized mean velocity contours $U/U_\infty$ and $V/U_\infty$ for the three height configurations. The space is normalized by canopy height $H$, gray bars mark panel location within the domain, and re-circulation regions are outlined by white dashed lines.

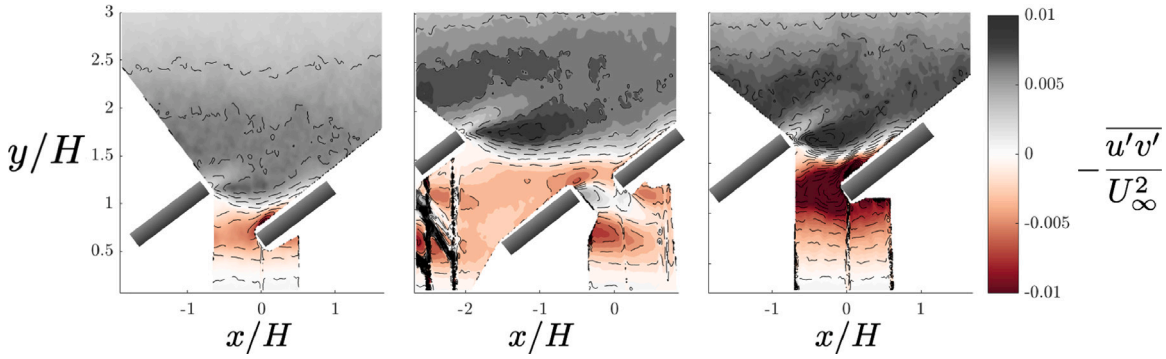


**Fig. 6.** Normalized Reynolds shear stress contours for $-\overline{u'v'}/U_\infty^2$ at the three height configurations ($Re = 6900$). Flow from left. Domain normalized by canopy height $H$ in both directions.

### 3.3. Turbulence flow field characteristics

As a primary driver in forced convection, turbulent mixing enhances heat transfer by thinning the panel surface boundary layer and increasing thermal shedding. Contours in Fig. 6 represent local turbulent mixing through Reynolds shear stress $-\overline{u'v'}/U_\infty^2$, where the prime symbol represents fluctuations of instantaneous velocity $u$ about the mean velocity ($u' = u - U$) and an overline denotes averaging in time.

For the NM case, the lower panel edge and the upper trailing edge are the most affected locations, where shearing is induced upon impact with the panel and at the top of the wake. More extreme values enclosing panel surfaces for the HM configuration represent the higher momentum exchange and turbulent mixing contributing to increased heat transfer. However, the shearing region near the SM shorter panel surface encompasses more space around the panels, with lower magnitudes along the panel surfaces than NM or HM. Along with the results seen in Fig. 5, this suggests that the slower sub-array flow and larger wake region provoke less efficiency in terms of moving the fluid and evacuating heat from the panel surface. The higher momentum entrainment above the array is more effective for removing heat from the taller panel surfaces than for the lower panels. It is possible that raising the entire array to allow for more fast-moving flow below the lower panels, or increasing the spacing behind the taller panels as done in industry, would improve the exchange of momentum across all panels withing the farm. For the HM array, intensified magnitudes of $-\overline{u'v'}/U_\infty^2$ are concentrated just above the array and at the panel lower edge, highlighting the turbulent mixing responsible for superior heat transfer among the three cases.

For canopy flow, $-\overline{u'v'}$ signifies local turbulent mixing due to flow interaction with a given body [42]. The sign of which indicates the direction of this momentum exchange. For example, the negative (red) regions in the shear stress contours of Fig. 6 imply that vertical and streamwise fluctuations share the same sign (e.g. $u' > 0$, $v' > 0$), a positive (gray) value denotes opposing signs, and the white separation indicates the region of near-zero velocity fluctuations. Viewing

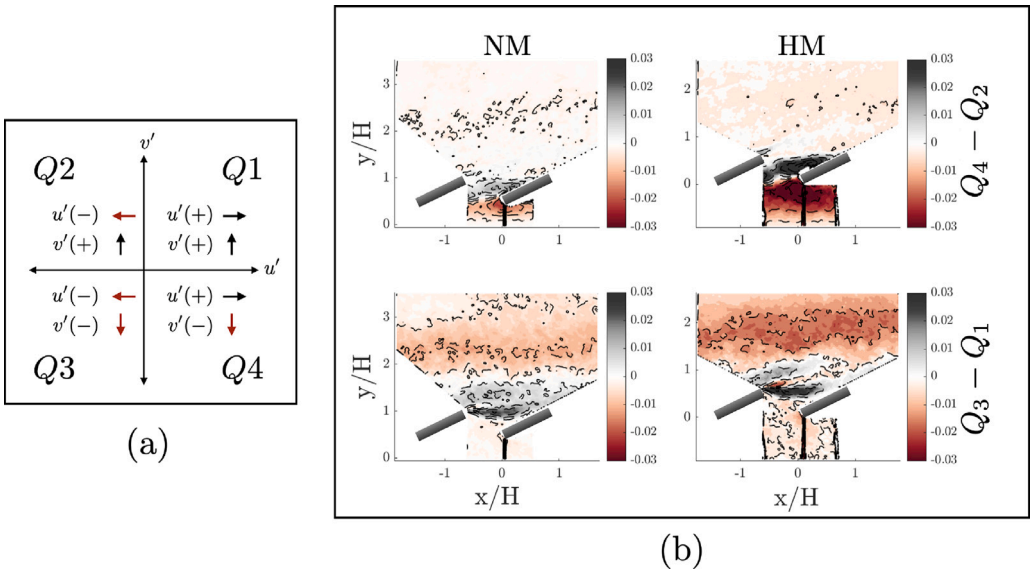


**Fig. 7.** Quadrant analysis explained and applied: (a) Quadrant descriptions for Reynolds shear stress $\overline{u'v'}$; (b) Comparative quadrants $Q_4 - Q_2$ (top) and $Q_3 - Q_1$ (bottom) for NM (left) and HM array cases (right).

momentum this way is historically discussed in terms of quadrant analysis [43,44]. In this method, the quantity of $\overline{u'v'}$ is classified into four unique flow events based on the sign of the fluctuating quantities as shown in Fig. 7(a).

For boundary layer flow, events in Quadrants 2 ($Q_2$) and 4 ($Q_4$) are regarded as ejections and sweeps, respectively, while Quadrants 1 ($Q_1$) and 3 ($Q_3$) represent outward and inward interactions [45]. For example, regions where $v'$ is positive ($Q_1$ and $Q_2$) represent an upward expulsion from the canopy, and a negative $v'$ denotes downward flow. Generally for canopy flow, sweeps and ejections are most prevalent in high momentum transport regions, where sweeps are most dominant within and just above the canopy [43]. Fig. 7(b) compares these events for the NM and HM cases, where the top row represents the difference between sweeps and ejections ($Q_4 - Q_2$) and the lower row compares inward *versus* outer interactions. Since $Q_4$ and $Q_2$ are inherently negative quantities, regions where $Q_4 - Q_2 < 0$ represent sweep dominance and $Q_4 - Q_2 > 0$ represent ejection dominance. Similarly for $Q_3 - Q_1$, a positive value denotes dominance of inward events while $Q_3 - Q_1 < 0$ points to more outward interactions. For NM, sweeps are most prevalent near the panel surface, and inward interactions are visible just after the panel trailing edge. Yet, the relatively moderate magnitudes compared to HM throughout the visible contour plane suggest that these events contribute less individually to convective mixing than in the higher panel case. For HM, sweeps significantly dominate for a majority of the region beneath the panels, while ejections at the panel surfaces are visible just under canopy height. The dominance of sweep events within the solar farm resembles behavior of urban and vegetative canopy flows such as forests and crop fields [43,46]. However, the ejection events present below the panel height highlight unique flow-altering characteristics of PV array geometries versus other canopy types [47,48]. For example, heat-shedding flow within an urban canopy is limited by the ground-to-canopy-top bluff building structures, whereas a PV array benefits from flow beneath the panel structures as well [31,42]. These varied interaction types are properties that also separate sparse from dense canopies, where the energetic flow behavior differs based on body-flow interaction [49].

### 3.4. Mean kinetic energy budgets

The nature of the flow within a solar farm can be directly described in terms of an energy balance, where the system is discussed separately in terms of inertia, energy produced, and energy transferred. From this perspective, the mean kinetic energy (MKE) highlights the mechanisms responsible for increasing/decreasing panel convection. The mean kinetic energy $K = 1/2U_i^2$, equation can be written as

$$U_j \frac{\partial K}{\partial x_j} = -\frac{\partial}{\partial x_j}(\overline{u_i' u_j'} U_i) + (\overline{u_i' u_j'}) \frac{\partial U_i}{\partial x_j}. \tag{3.1}$$

The subscripts $i$ and $j$ denote tensor notation and refer to streamwise and wall-normal directions when applied to either domain $(x, y)$ or velocities $(u, v)$. Since the flow field being considered is sufficiently far from any surfaces, the MKE viscous dissipation term is considered negligible. The physical meaning of each term can be discussed in general fashion. The inertial term ($\mathcal{I}_M = U_j \frac{\partial K}{\partial x_j}$) describes the advection of mean kinetic energy by the wind. The transport term ($\mathcal{T}_M = \frac{\partial}{\partial x_j}(\overline{u_i' u_j'} U_i)$) describes the flux due to turbulent stresses. The production term ($\mathcal{P} = (\overline{u_i' u_j'}) \frac{\partial U_i}{\partial x_j}$) describes energy transferred from mean velocity to the turbulence.

Fig. 8 shows normalized horizontally-averaged values of the MKE terms of the energy budget for the NM and HM array configurations. The vertical $y$ locations are normalized by the height of the lower panel edge of the nominal array (e.g. $B_{*,NM} = B_{NM}$) to allow ease of comparison relative to the panel region. The general shape of the MKE budget profiles is similar between the NM and HM arrays, and mimics the behavior seen for Reynolds shear stress in Fig. 6, with HM values being larger than those of the NM array. This result is due to a decrease in flow blockage between the panel rows when the height is doubled, leading to increased flow especially underneath the panels. In both cases, the major terms are production and energy transport. The advection term is marginal for the NM case as a result of more flow homogeneity. Interestingly, the greatest advection term is found at the lower panel edge. The panels enhance the flow circulation and induce flow heterogeneity. For the mean production term, the greatest of these losses is also at the lower edge in both arrays. For the mean transport term, the negative values above and below the array indicate MKE being entrained into the panel region, with notably greater contributions coming from the inner region in the HM array. The magnitudes for the HM array are about twice those of the nominal array, highlighting the root of augmented heat transfer shown in the $Nu$ values (Fig. 4). This implies that the disparity between the arrays is due to a significant boost in momentum from below the panels, which also aligns with the dominant sweep events from Fig. 7, shedding heat from the rear surfaces.

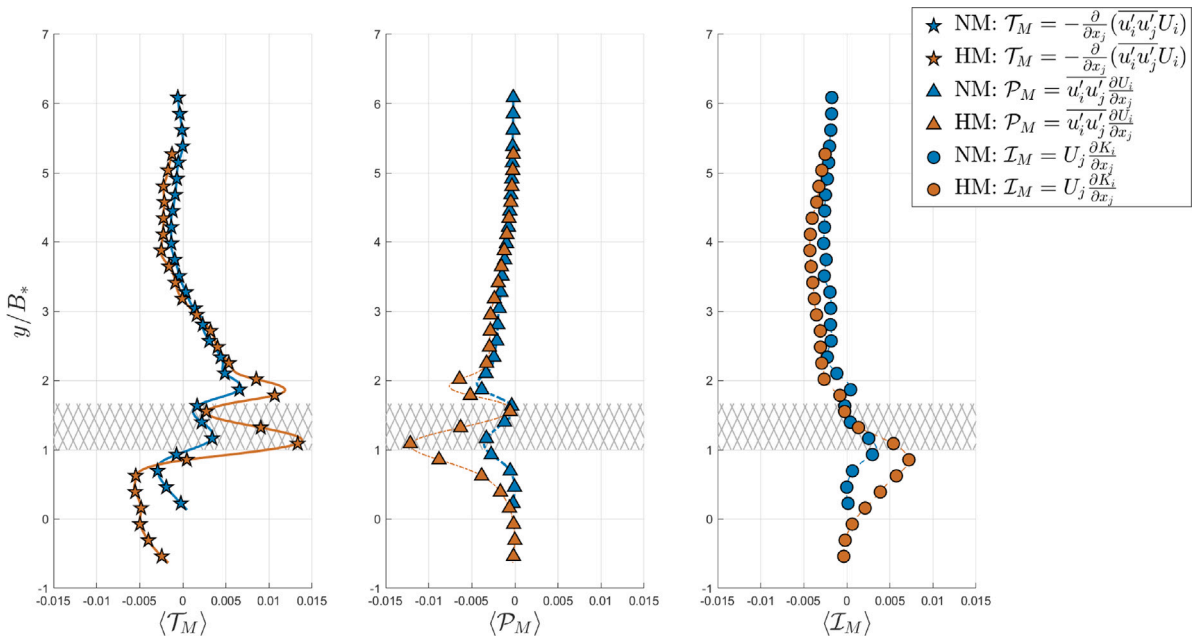


**Fig. 8.** Vertical profiles of term contributions to mean kinetic energy - Left: Transport ($\mathcal{T}_M$), Middle: Production ($\mathcal{P}_M$), and Right: Inertial ($\mathcal{I}_M$) - for NM and HM configurations (teal and orange respectively).

## 4. Conclusions

Solar farm cooling in forced convection is enhanced by panel height and the resulting entrainment of high energy flow within the array. For a given inflow velocity, the high mount (HM) panels produced improvements on $Nu_{H_{xM}}$ over 1.88 times that of the nominal case (NM) due to increased sub-panel space encouraging higher velocity flow under the array while benefiting from increased turbulent mixing above the panels. For each configuration, re-circulation downstream of the panels inhibits convection from the panel rear surface, but increased array height allows for fast-moving sub-array flow to be pulled upward to aid with convection. Due to wind-panel interaction, the region is separated into a sub-array flow layer, a deficit-producing region due to panel blockage, and ultimately an above-panel outer layer. In the staggered (SM) height array, undulation of the outer, cooler, high-momentum flow entering the upper part of the array increases cooling for the taller panel surfaces, but the induced blockage, slower sub-panel velocities and re-circulation within the canopy keep the warmer air nearer to the panels. It is assumed that raising the lower panels, or the entire array, may allow for faster flow to interact with the panels and remove more heat from the surface.

Mean kinetic energy (MKE) and quadrant analysis of the two extreme height cases, NM and HM, highlight the enhancing role of energy exchange in heat transfer. Overall, MKE term magnitudes for the HM array are nearly twice greater than for NM due to reduced panel interaction and faster sub-panel flow. Advection plays a minor role in terms of the MKE budget for both cases, likely due to the more homogeneous flow compared to SM. However, peaks in advection at the panel leading edge speak to the introduction of heterogeneity due to module presence. Energy loss shown through the production term is greatest at panel leading edges, while transport indicates energy entrainment toward the panels from higher velocity flow.

Collectively, the presented work offers an energetic perspective on solar array height changes and their effect on forced convection within large-scale PV plants. Considering the complicated and varied environments these systems inhabit, the discussed results motivate future investigation in balancing configuration-induced production increases and complicated coupling effects of operating plants such as force loading, unsteady or absent winds, and variable-tilt systems. For example, the simplified parameters herein – *i.e.* fixed-tilt modules under constant, uni-directional, and non-zero wind flow – represent a small subset of conditions from which more exhaustive studies would benefit by branching beyond. Furthermore, any solution for new or operating PV designs must consider relative costs of module manufacturing, installation and ongoing maintenance. Whether the increased energy output due to plant changes, such as module height, outweigh these costs must be examined through techno-economic framework to fully gauge functional feasibility.

### CRediT authorship contribution statement

**Sarah E. Smith:** Data acquisition, Data curation, Formal analysis, Writing – original draft, Writing – review & editing. **Bianca Viggiano:** Data acquisition, Data curation, Formal analysis, Writing – original draft, Writing – review & editing. **Naseem Ali:** Conceptualization, Data acquisition, Data curation, Formal analysis, Writing – original draft, Writing – review & editing. **Timothy J Silverman:** Writing – review & editing. **Marc Calaf:** Conceptualization, Writing – review & editing. **Raúl Bayoán Cal:** Conceptualization, Writing – review & editing.

### Declaration of competing interest

The authors declare the following financial interests/personal relationships which may be considered as potential competing interests: Raul Bayoan Cal reports financial support was provided by US Department of Energy. Timothy J Silverman reports financial support was provided by Office of Energy Efficiency and Renewable Energy.

### Data availability

Data will be made available on request.

### Acknowledgments

This work is based upon work supported by the U.S. Department of Energy Office of Energy Efficiency and Renewable Energy Solar Energy Technologies Office, under Award Number DE-EE0008168, and was authored in part by the National Renewable Energy Laboratory, operated by Alliance for Sustainable Energy, LLC, for the U.S. Department

of Energy (DOE) under Contract No. DE-AC36-08GO28308. Funding provided by U.S. Department of Energy Office of Energy Efficiency and Renewable Energy Solar Energy Technologies Office. The views expressed in the article do not necessarily represent the views of the DOE or the U.S. Government. The U.S. Government retains and the publisher, by accepting the article for publication, acknowledges that the U.S. Government retains a nonexclusive, paid-up, irrevocable, worldwide license to publish or reproduce the published form of this work, or allow others to do so, for U.S. Government purposes.

## References

[1] The International Renewable Energy Agency. Renewable energy statistics 2020. Technical Report, IRENA; 2020.
[2] US Energy Information Administration. Electric power monthly. Technical Report, EIA; 2021.
[3] Dupré O, Vaillon R, Green M. Physics of the temperature coefficients of solar cells. Sol Energy Mater Sol Cells 2015;140:92–100. http://dx.doi.org/10.1016/j.solmat.2015.03.025.
[4] Wysocki JJ, Rappaport P. Effect of temperature on photovoltaic solar energy conversion. J Appl Phys 1960;31(3):571–8. http://dx.doi.org/10.1063/1.1735630.
[5] Skoplaki E, Palyvos J. On the temperature dependence of photovoltaic module electrical performance: A review of efficiency/power correlations. Sol Energy 2008;83(5):614–24. http://dx.doi.org/10.1016/J.SOLENER.2008.10.008.
[6] Muller M. Measuring and modeling nominal operating cell temperature (NOCT). Technical Report, NREL; 2010.
[7] King DL, Kratochvil JA, Boyson WE. Field experience with a new performance characterization procedure for photovoltaic arrays. Technical Report, Albuquerque, NM (US): Sandia National Labs.; 1997.
[8] Chow TT, Pei G, Fong K, Lin Z, Chan A, Ji J. Energy and exergy analysis of photovoltaic–thermal collector with and without glass cover. Appl Energy 2009;86(3):310–6. http://dx.doi.org/10.1016/j.apenergy.2008.04.016.
[9] Bahaidarah H, Subhan A, Gandhidasan P, Rehman S. Performance evaluation of a PV (photovoltaic) module by back surface water cooling for hot climatic conditions. Energy 2013;59:445–53. http://dx.doi.org/10.1016/j.energy.2013.07.050.
[10] Zhang X, Zhao X, Xu J, Yu X. Characterization of a solar photovoltaic/loop-heat-pipe heat pump water heating system. Appl Energy 2013;102:1229–45. http://dx.doi.org/10.1016/j.apenergy.2012.06.039.
[11] Teo HG, Lee PS, Hawlader M. An active cooling system for photovoltaic modules. Appl Energy 2012;90(1):309–15. http://dx.doi.org/10.1016/j.apenergy.2011.01.017.
[12] Beatty B, Macknick J, McCall J, Braus G, Buckner D. Native vegetation performance under a solar PV array at the national wind technology center. Technical Report, NREL; 2017.
[13] Dinesh H, Pearce JM. The potential of agrivoltaic systems. renewable sustainable energy rev 2016;54:299–308. . http://dx.doi.org/10.1016/j.rser.2015.10.024.
[14] Adeh EH, Good SP, Calaf M, Higgins CW. Solar PV power potential is greatest over croplands. Sci Rep 2019;9:11442. http://dx.doi.org/10.1038/s41598-019-47803-3.
[15] Gupta S, Anand P, Kakkar S, Sagar P, Dubey A. Effect of evapotranspiration on performance improvement of photovoltaic- green roof integrated system. Int J Renewable Energy 2017;12:13.
[16] Steadman C, Higgins C. Agrivoltaic systems have the potential to meet energy demands of electric vehicles in rural Oregon, US. Sci Rep 2022;12. http://dx.doi.org/10.1038/s41598-022-08673-4.
[17] Adeh E, Selker J, Higgins C. Remarkable agrivoltaic influence on soil moisture, micrometeorology and water-use efficiency. PLoS One 2018;13. http://dx.doi.org/10.1371/journal.pone.0203256.
[18] Krishnamurthy A, Serpell O. Harvesting the sun: On-farm opportunites and challenges for solar development. Technical Report, Kleinman Center for Energy Policy; 2021.
[19] Loughner CP, Allen DJ, Zhang D-L, Pickering KE, Dickerson RR, Landry L. Roles of urban tree canopy and buildings in urban heat island effects: Parameterization and preliminary results. J Appl Meteorol Climatol 2012;51:1775–93. http://dx.doi.org/10.1175/JAMC-D-11-0228.1.
[20] Stanislawski BJ. Influence of spatial arrangement of solar farms in convective cooling and module temperature. PhD Thesis, University of Utah 2021; [In Press].
[21] Glick A, Ali N, Bossuyt J, Calaf M, Cal RB. Utility-scale solar PV performance enhancements through system-level modifications. Sci Rep 2020;10(1):1–9. http://dx.doi.org/10.1038/s41598-020-66347-5.
[22] Cheng C, Chung P, Yang R. Wind loads on a solar panel at high tilt angles. Appl Sci 2019;9:1594. http://dx.doi.org/10.3390/app9081594.
[23] Sparrow E. Effect of finite width on heat transfer and fluid flow about an inclined rectangular plate. J Heat Transfer 1979;101:199. http://dx.doi.org/10.1115/1.3450946.
[24] Sparrow E, Niethammer J, Chaboki A. Heat transfer and pressure drop characteristics of arrays of rectangular modules encountered in electronic equipment. Int J Heat Mass Transfer 1982;25(7):961–73. http://dx.doi.org/10.1115/1.3244250.
[25] Test F, Lessmann R, Johary A. Heat transfer during wind flow over rectangular bodies in the natural environment. J Heat Transfer 1981;103(2):262–7. http://dx.doi.org/10.1115/1.3244451.
[26] Kind R, Gladstone D, Moizer A. Convective heat losses from flat-plate solar collectors in turbulent winds. J Sol Energy Eng 1983;105:80–5. http://dx.doi.org/10.1115/1.3266350.
[27] Karava P, Jubayer CM, Savory E. Numerical modelling of forced convective heat transfer from the inclined windward roof of an isolated low-rise building with application to photovoltaic/thermal systems. Appl Therm Eng 2011;31(11–12):1950–63. http://dx.doi.org/10.1016/j.applthermaleng.2011.02.042.
[28] Kaplani E, Kaplanis S. Thermal modelling and experimental assessment of the dependence of pv module temperature on wind velocity and direction, module orientation and inclination. Sol Energy 2014;107:443–60. http://dx.doi.org/10.1016/J.SOLENER.2014.05.037.
[29] Sartori E. Convection coefficient equations for forced air flow over flat surfaces. Sol Energy 2006;80(9):1063–71. http://dx.doi.org/10.1016/j.solener.2005.11.001.
[30] Arianmehr I. Turbulence convective heat transfer for cooling the photovoltaic cells. Electronic Theses and Dissertations, University of Windsor 2014:5149. https://scholar.uwindsor.ca/etd/5149.
[31] Glick A, Smith SE, Ali N, Bossuyt J, Recktenwald G, Calaf M, Cal RB. Influence of flow direction and turbulence intensity on heat transfer of utility-scale photovoltaic solar farms. Sol Energy 2020;207:173–82. http://dx.doi.org/10.1016/j.solener.2020.05.061.
[32] Smith SE, Glick A, Ali N, Bossuyt J, McNeal J, Recktenwald G, Calaf M, Cal RB. Configuration effects on flow dynamics and convective behavior in large-scale solar arrays. In: 2020 47th IEEE photovoltaic specialists conference (PVSC). 2020, p. 2195–6. http://dx.doi.org/10.1109/PVSC45281.2020.9300740.
[33] King DL, Kratochvil JA, Boyson WE. Temperature coefficients for PV modules and arrays: measurement methods, difficulties, and results. In: Conference record of the twenty sixth IEEE photovoltaic specialists conference-1997. IEEE; 1997, p. 1183–6. http://dx.doi.org/10.1109/PVSC.1997.654300.
[34] Fuentes M. A simplified thermal model of photovoltaic modules. Technical Report, Albuquerque, NM (US): Sandia National Labs.; 1985.
[35] Kratochvil J, Boyson W, King D. Photovoltaic array performance model. Technical Report, United States: Sandia National Labs; 2004, http://dx.doi.org/10.2172/919131.
[36] Vaillon R, Dupré O, Cal RB, Calaf M. Pathways for mitigating thermal losses in solar photovoltaics. Sci Rep 2018;8(1):13163. http://dx.doi.org/10.1038/s41598-018-31257-0.
[37] Glick A, Ali N, Bossuyt J, Recktenwald G, Calaf M, Cal RB. Infinite photovoltaic solar arrays: Considering flux of momentum and heat transfer. Renew Energy 2020;156:791–803. http://dx.doi.org/10.1016/j.renene.2020.03.183.
[38] Average wind speeds - map viewer. NOAA 2022. https://www.climate.gov/maps-data/dataset/average-wind-speeds-map-viewer.
[39] Incropera F, Lavine A, Bergman T, DeWitt D. Fundamentals of heat and mass transfer. Wiley; 2007.
[40] Dupré O, Vaillon R, Green MA. Thermal behavior of photovoltaic devices. In: physics and engineering. Cham, Switzerland: Springer; 2017, http://dx.doi.org/10.1007/978-3-319-49457-9.
[41] Otth DH, Ross RG. Assessing photovoltaic module degradation and lifetime from long term environmental tests. 29th Institute of Environmental Sciences Technical Meeting, Los Angeles, CA 1983;121–26.
[42] Böhm M, Finnigan JJ, Raupach MR, Hughes D. Turbulence structure within and above a canopy of bluff elements. Boundary Layer Meteorol 2013;146:393–419. http://dx.doi.org/10.1007/s10546-012-9770-1.
[43] Brunet Y. Turbulent flow in plant canopies: Historical perspective and overview. Boundary-Layer Meteorol 2020;177:315–64. http://dx.doi.org/10.1007/s10546-020-00560-7.
[44] Kadum HF, Knowles D, Cal RB. Quantification of preferential contribution of Reynolds shear stresses and flux of mean kinetic energy via conditional sampling in a wind turbine array. J Fluids Eng 2018;141. http://dx.doi.org/10.1115/1.4040568.
[45] Wallace JM. Quadrant analysis in turbulence research: History and evolution. Annu Rev Fluid Mech 2016;48(1):131–58. http://dx.doi.org/10.1146/annurev-fluid-122414-034550.
[46] Finnigan JJ. Chapter Two - The turbulent wind in plant and forest canopies. In: Johnson EA, Miyanishi K, editors. Plant disturbance ecology. San Diego: Academic Press; 2021, p. 17–63. http://dx.doi.org/10.1016/B978-0-12-818813-2.00002-2.
[47] Yue W, Meneveau C, Parlange MB, Zhu W, van Hout R, Katz J. A comparative quadrant analysis of turbulence in a plant canopy. Water Resour Res 2007;43(5). http://dx.doi.org/10.1029/2006WR005583.
[48] Boppana VBL, Xie Z-T, Castro IP. Thermal stratification effects on flow over a generic urban canopy. Boundary Layer Meteorol 2014;153:141–62. http://dx.doi.org/10.1007/s10546-014-9935-1.
[49] Katul GG, Mahrt L, Poggi D, Sanz C. ONE- and TWO-equation models for canopy turbulence. Boundary Layer Metereol 2004;113:81–109. http://dx.doi.org/10.1023/B:BOUN.0000037333.48760.e5.